

See discussions, stats, and author profiles for this publication at: <https://www.researchgate.net/publication/231650377>

A Photoemission Study of the Morphology and Barrier Heights of the Interface between Chrysene and Inert Substrates

ARTICLE *in* THE JOURNAL OF PHYSICAL CHEMISTRY C · JANUARY 2009

Impact Factor: 4.77 · DOI: 10.1021/jp803958e

CITATIONS

10

READS

23

3 AUTHORS:



Bengt Jaeckel

UL

36 PUBLICATIONS 261 CITATIONS

[SEE PROFILE](#)



Justin Sambur

Cornell University

17 PUBLICATIONS 708 CITATIONS

[SEE PROFILE](#)



Bruce A Parkinson

University of Wyoming

251 PUBLICATIONS 7,087 CITATIONS

[SEE PROFILE](#)

Article

A Photoemission Study of the Morphology and Barrier Heights of the Interface between Chrysene and Inert Substrates

B. Jaeckel, J. Sambur, and B. A. Parkinson

J. Phys. Chem. C, **2009**, 113 (5), 1837-1849 • DOI: 10.1021/jp803958e • Publication Date (Web): 08 January 2009

Downloaded from <http://pubs.acs.org> on April 9, 2009

More About This Article

Additional resources and features associated with this article are available within the HTML version:

- Supporting Information
- Access to high resolution figures
- Links to articles and content related to this article
- Copyright permission to reproduce figures and/or text from this article

[View the Full Text HTML](#)



ACS Publications

High quality. High impact.

The Journal of Physical Chemistry C is published by the American Chemical Society. 1155 Sixteenth Street N.W., Washington, DC 20036

A Photoemission Study of the Morphology and Barrier Heights of the Interface between Chrysene and Inert Substrates

B. Jaeckel, J. Sambur, and B. A. Parkinson*,†

Department of Chemistry, Colorado State University, Fort Collins, Colorado 80523

Received: May 05, 2008; Revised Manuscript Received: October 17, 2008

Chrysene, a two-dimensional (2D) chiral isomer of tetracene, was deposited onto inert metallic (Au(111), Cu(111), Ag(111), and highly oriented pyrolytic graphite (HOPG)) and semiconducting (SnS₂) substrates with hexagonal symmetry. The interface formation was investigated *in situ* with photoelectron spectroscopy (X-ray photoelectron spectroscopy and UV photoelectron spectroscopy (UPS)). A detailed analysis of core-level and valence band spectra revealed that the barrier height for holes or electrons is independent of the identity and work function of the metal substrate. Metal/chrysene interfaces are therefore an example of pure Fermi level pinning where changes in the interface dipole potential directly offset changes in the metal work function. The results provide evidence that the pinning may result from a hybridization mechanism between metal s states and organic π states. UPS spectra indicate that the 2D structures of the chrysene wetting layer is different for high work function materials (Au(111), SnS₂) compared to low work function materials (Ag(111) and HOPG). Stranski-Krastanov growth was observed on all substrates and is in agreement with optical microscope images of thick chrysene films.

I. Introduction

The fundamental physics describing the formation of Schottky barriers/contacts for inorganic semiconductor metal contacts has been studied and debated for decades.^{1–9} In recent years organic semiconductors have become a major research field due to their successful application in optical and electronic devices. Devices such as organic light emitting diodes and organic thin film transistors have been demonstrated, and their performance has rapidly improved.^{10–13} Therefore the fundamental aspects of metal contacts to these organic semiconductors becomes of vital importance since it will determine the eventual device performance.

The interfaces at both the front and back contacts are crucial for device performance. The most highly studied organic/metal system is the metal/pentacene interface since pentacene exhibits the highest charge carrier mobilities among organic semiconductors. Electronic properties of the interface have been mostly studied using photoelectron spectroscopies (X-ray photoelectron emission spectroscopy (XPS) and ultraviolet photoelectron emission spectroscopy) and current–voltage (I – V) measurements. The detailed surface morphology is usually investigated with scanning tunneling microscopy (STM) for real space imaging or with low-energy electron diffraction (LEED) for reciprocal space information. Different two-dimensional (2D) structures have been observed in the sub- and monolayer regimes for pentacene on Au(111),^{14–17} while on other substrates with the same symmetry quite different structures were found (e.g., pentacene on Ag/Si(111)).^{18,19} With change of the symmetry of the substrate, other 2D structures can be templated (e.g., pentacene on Cu(110)).^{20–22}

Photoelectron spectroscopy studies of the electronic interfacial properties of metal/organic contacts yield detailed band energy

line-ups between the HOMO and LUMO levels of the organic semiconductors and the Fermi level of the metal. In most cases of polyaromatic hydrocarbons (PAHs) adsorbed on metals, an interface dipole potential δ is formed^{23–29} that can influence the formation of different surface structures. In most cases the measured dipole potential is a linear function of the substrate work function^{27,30} with slopes varying from 0.5 to 1.0, where 1.0 describes pure Fermi level pinning. Rather than plotting the interface dipole potential δ versus substrate work function, a plot of the barrier height for holes or electrons versus substrate work function yields the slope parameter S . When an interface is Fermi level pinned ($S = 0$) the hole or electron injection barriers are only slightly (if at all) changed when varying the metal work function. Pentacene contacts with various metals demonstrate $S = 0.36$ as determined by both I – V ³⁰ and XPS measurements.^{27,28,31} Pure Fermi level pinning is referred to as the Bardeen limit ($S = 0$), whereas the Schottky limit describes the situation where the barrier height tracks the work function of the metal ($S = 1$).

To get a better understanding of the relationship between electronic properties and interface morphology (first monolayer and the 2D structure), we studied the electronic properties of chrysene interfaces with different substrates using photoelectron spectroscopy. The choice of chrysene has two interesting aspects: (1) it is a small polyaromatic hydrocarbon (PAH) that is an isomer of tetracene and (2) it is a 2D chiral molecule (see Figure 1b). Monolayers can possess domains of chirality as was demonstrated for a similar 2D chiral molecule PAH, naphthalo[2,3-*a*]pyrene on Au(111).²⁶

In this contribution we will focus on the electronic interface properties of chrysene on the metallic substrates Au(111), Cu(111), Ag(111), and highly ordered pyrolytic graphite (HOPG) and on semiconducting SnS₂ to demonstrate whether chrysene is an example of the Bardeen limit or the Schottky limit for semiconductor/metal contacts. These substrates were chosen because they are nonreactive with PAH molecules,

* Corresponding author. Bruce.Parkinson@colostate.edu.

† Present address: Department of Chemistry and School of Energy Resources, University of Wyoming, Laramie, WY 82071. E-mail: bsparkin1@uwyo.edu.

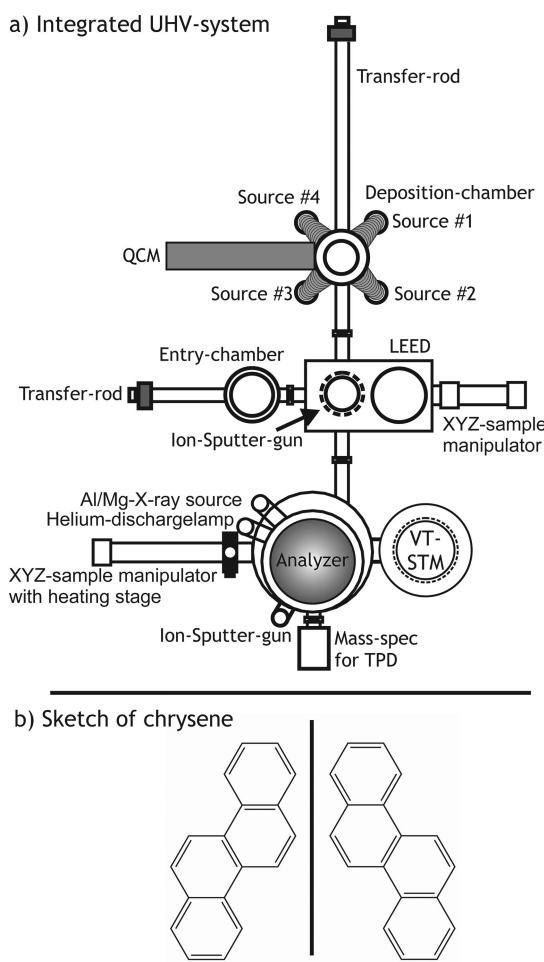


Figure 1. (a) Schematic representation of the used UHV system and (b) a sketch of chrysene, the molecule used in this study with the two possible enantiomers in a 2D environment.

exhibit hexagonal symmetry, vary widely in work function and may be prepared with large atomically flat areas.

II. Experimental Setup

The experiments were performed in a commercial Omicron Multiprobe ultrahigh vacuum (UHV) system with a base pressure of 5×10^{-10} mbar (see Figure 1a). The system is equipped with variable-temperature scanning tunneling microscopy (VT-STM), low-energy electron diffraction (LEED), and X-ray and ultraviolet photoelectron spectroscopies (XPS and UPS). Electron detection is achieved using a VSW EA125 single-channel hemispherical analyzer. Binding energies are calibrated to the Fermi edge and to literature values of the Au 4f, Ag 3d, and Cu 2p core level emissions.

Chrysene (see Figure 1b), obtained from Aldrich in the highest purity grade, was deposited by physical vapor deposition in a home-built oil bath source with a source temperature of ≈ 115 °C, leading to a deposition rate of ≈ 7 – 9 Å/min. During deposition the pressure in the deposition chamber was usually lower than 1×10^{-8} mbar. After deposition, the sample was transferred *in situ* to the analysis chamber for immediate photoemission measurements.

Approximately 200–300 nm thick gold, copper, and silver films were deposited on mica substrates heated to ≈ 200 °C. After several sputtering (Ar ions with energies of 800–1500

V) and annealing steps (several hours at 250–350 °C), large and nearly defect free (111) terraces were formed.

HOPG and SnS₂, both layered materials, were cleaved in air with Scotch tape and immediately introduced into the vacuum system. This procedure yielded substrates nearly free of defects and adventitious hydrocarbons. Prior to deposition of chrysene the layered substrates were heated to ~ 200 °C to desorb any contaminates.

XPS and UPS were used to verify the cleanliness of the surfaces prior to chrysene deposition. UPS valence band spectra and work functions (calculated from the secondary electron onset SEO) accurately reflected literature values, and only negligible carbon signals were detected by XPS before chrysene deposition (except for HOPG).

In all experimental results, thicknesses are reported in angstroms and are calculated via total deposition time in conjunction with the deposition rate (typically ≈ 8 Å/min) measured using a quartz microbalance. Although charging is visible in XPS, and especially in UPS, we were not able to prepare a uniformly thick film. In some areas the film thickness never exceeded three to four monolayers. The number of monolayers corresponds to the escape depth of photoelectrons from the substrate by assuming a monolayer chrysene thickness of 6 Å (which is the average of flat-lying, short- or long-edge tilted molecules). The substrate signals should be suppressed when the chrysene coverage approaches three to four monolayers.

A careful fitting procedure was performed on all photoemission data using Wavemetrics IGOR PRO software. The Au 4f, Ag 3d, Sn 3d, and S 2p emissions were fit with a single component and a doublet of a Gaussian–Lorentzian function with a constant energy splitting. Depending on the coverage, the C 1s emission was fit with a single Gaussian–Lorentzian function (low coverages) and with a multiple peak function for higher coverages including the high binding energy asymmetry that is due to charging of the growing chrysene film. The Cu 2p_{3/2} emission is only shown here since the splitting of the 3/2 and the 1/2 is quite large (19.8 eV), and a background removal over this range is not possible. Therefore the 3/2 and the 1/2 were background subtracted and fitted separately, and the results were consistent.

An approximate value for the band gap of chrysene of 3.4 eV was determined from the optical band gap obtained with UV-vis spectroscopy (see Figure 2). The spectrum was background-corrected using a polynomial function. The spectrum was taken from a thick chrysene film, deposited onto a quartz plate with another clean quartz plate used as reference. The lowest energy adsorption maximum was used as an estimate for the band gap. This value probably overestimates the band gap, but the use of the strong sharp absorption maximum gives an unambiguous and reproducible value in comparison to applying the value for the onset optical absorbance. The different adsorption maxima in the spectrum are due to different allowed π – π^* transitions.

III. Experimental Results

We will separate this section by substrates and present the detailed experimental results for each substrate. We will start with the metal substrates and proceed according to descending work functions. Finally we present the results on the layered semiconductor SnS₂.

A. Deposition onto Au(111). XPS and UPS spectra are shown in Figures 3 and 4, respectively. Figure 4b illustrates the normalized integrated area intensities for the Au 4f and the C 1s emissions from Figure 3, panels a and b. After ap-

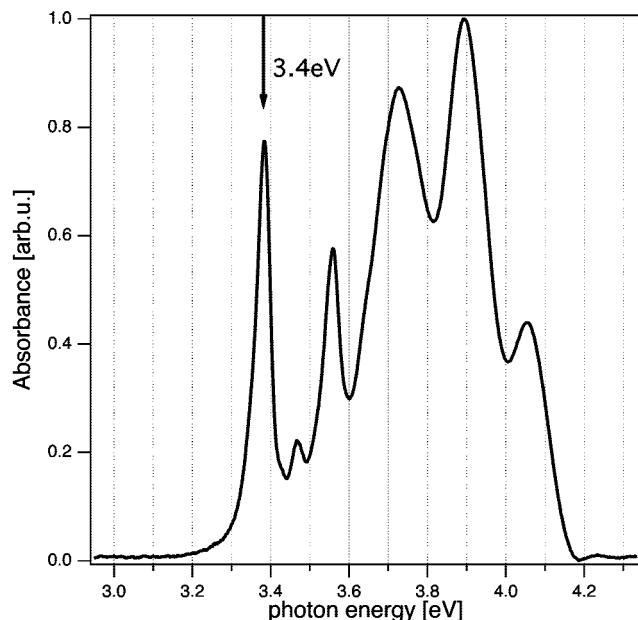


Figure 2. Optical absorption spectra of a thick chrysene film deposited on quartz and used to estimate the band gap. The first adsorption maximum at ≈ 3.4 eV was chosen as the band gap value for chrysene.

proximately 35 Å was deposited (see marker in Figure 4b), a change in growth mode occurs. Initially the Au 4f is strongly suppressed while a large increase in C 1s intensity is measured, indicating that gold is uniformly covered with chrysene. At very long deposition times only a small decrease in substrate intensity occurs, indicating that chrysene tends to form islands. We conclude therefore from the intensity change of the XPS core levels that chrysene grows on Au(111) in a Stranski–Krastanov growth mode where an initial wetting layer is followed by island growth.

The binding energy of the Au 4f emission, obtained after a careful fitting procedure, is constant at 84.0 eV (Figure 3c) for all deposition steps. Initially the binding energy of the C 1s is increasing. For organic semiconductor/high work function metal interfaces, this behavior is typically explained by screening effects in the first monolayers.^{23–29} The screening decreases with increasing film thickness and finally results in a constant binding energy for the C 1s level of the organic material. For intermediate coverages, a nearly constant binding energy of the C 1s of 284.6 eV was measured. For thicker films, as in the present case, charging can also lead to a shift to higher binding energies. To confirm that the shifts are related to charging, the binding energies were measured as a function of the excitation intensity by varying the power of the X-ray source. Different shifts were measured at higher intensities. Spectra of thick films, showing evidence of charging effects are shown, but these binding energy values are not used in our analysis.

Unfortunately, the evolution of the HOMO levels of chrysene in the UPS spectra on Au(111) are very difficult to evaluate. In the valence band region the Au 5d states³² overlap with the growing HOMO levels of chrysene. Since chrysene forms a wetting layer on Au(111), there is always an overlap of substrate and overlayer emissions at higher coverages, making it impossible to determine the HOMO cutoff position of chrysene. Fortunately, in the binding energy region between 8 and 10 eV, there are no prominent Au states and at higher chrysene coverages a new strong emission is visible (labeled HOMO_X in Figure 4a). UPS spectra collected for chrysene on HOPG,

where no prominent HOPG emission occurs between 0 and 10 eV (see especially Figure 10c) reveal an emission that can be attributed to a chrysene HOMO level. The constant binding energy of the chrysene emission on Au(111) in comparison with HOPG corroborates the XPS results, which provide no evidence for band bending in the thick chrysene film.

The formation of an interface dipole potential results from the absence of band bending and is revealed by the large change in the secondary electron onset in the UPS spectra (see Figure 4a). During the formation of the interface a work function change from ≈ 5.4 eV for the clean Au(111) substrate to ≈ 4.0 eV for the intermediately thick chrysene films was measured (see Figure 4c). The obtained value for the interface dipole potential of $\delta \approx 1.4$ eV is among the highest obtained for organic molecules on metallic substrates (for comparison: on Au(111) pentacene $\delta \approx 1.0$ eV,^{25,28} naphtho[2,3-*a*]pyrene $\delta \approx 1.0$ eV,²⁶ Alq₃ $\delta \approx 1.2$ eV).²³

The electronic interface properties of chrysene on Au(111) are summarized in a band energy diagram given in Figure 13a). The position of the HOMO cutoff (1.6 eV) was calculated from the HOMO_X position where 6.9 eV was subtracted (see HOPG results and Figure 10).

B. Deposition onto Cu(111). The experimental procedure for the deposition of chrysene onto Cu(111) was identical to the deposition on Au(111). XPS and UPS spectra are shown in Figures 5 and 6, respectively. For clarity we present only the Cu 2p_{3/2} emission since the 3/2 to 1/2 splitting is very large (19.8 eV). As one can expect, the binding energy of the metallic substrate is, within the experimental error, constant. Initially, there are only minor shifts to slightly higher binding energy in the C 1s leading to a C 1s binding energy of 284.7 eV, comparable to the value found on Au(111). The shift to higher binding energies at higher coverages is due to the strong charging observed for all chrysene films presented herein.

The intensities of the Cu 2p and the C 1s emissions determined from the XPS measurements are given in Figure 6b. The general trends in intensity are similar to Au(111). At a thickness of 15 Å, a change in growth mode is again apparent. Initially a wetting layer of chrysene is formed followed by island growth, consistent with the observation that after very long deposition times the copper emissions are still present. Therefore the growth mode for chrysene on Cu(111) can also be characterized as Stranski–Krastanov growth.

The UPS spectra provide information about the HOMO levels of chrysene and allow the evaluation of the trend in work function from the bare Cu(111) surface to the thick chrysene film. The clean Cu(111) surface shows the expected Cu 3d valence band states,³³ surface state, and a work function of 4.8 eV. The initial chrysene deposition induces a large change in work function (see Figure 6, panels a and c). After 15 Å was deposited, where the change in growth mode appears, the work function starts to level out. Unfortunately, the onset of charging effects prevents observation of a constant value for the work function. This is demonstrated by the broadening of the secondary electron onset (SEO) and the evolution of a second SEO. The conclusion from the evaluation of the SEO is that the work function of chrysene on Cu(111) is less than 4.2 eV.

The determination of the chrysene HOMO level emission near the Fermi level is hindered by the strong Cu 3d valence band emissions. In the binding energy region between 8 and 10 eV, prominent emissions are measured immediately after the first deposition step as was also observed on Au(111). These emissions are labeled HOMO_X in Figure 6. The low binding energy HOMO_X emission was determined at 8.7 eV with a

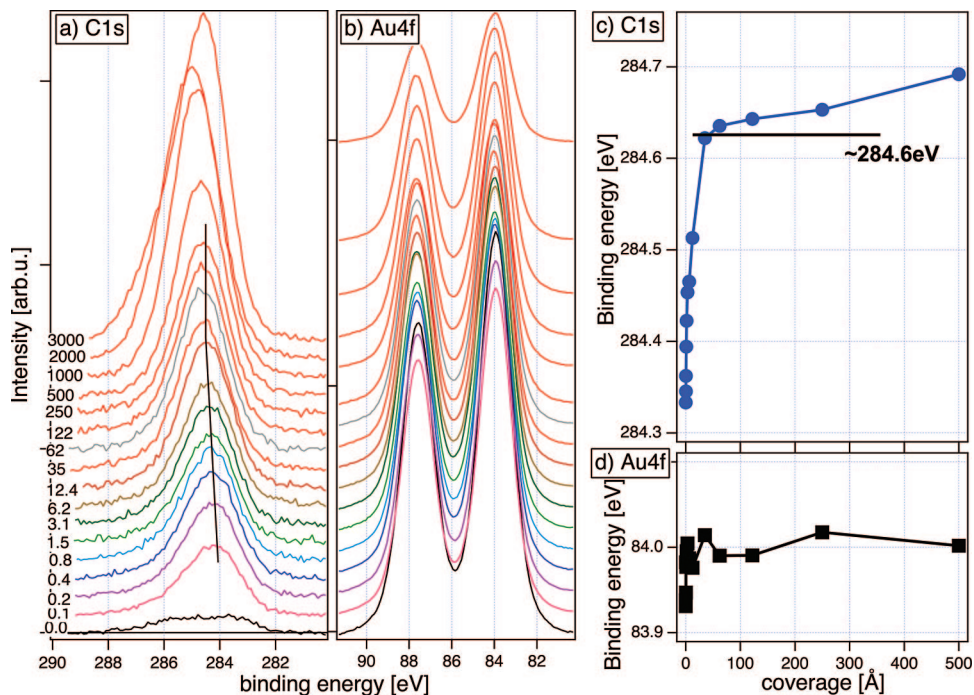


Figure 3. Collected XPS spectra and binding energy values during the deposition of chrysene on Au(111): (a) C 1s spectra, (b) Au 4f spectra. Fitted binding energy values are shown for the C 1s emission in (c) and for the Au 4f emission in (d).

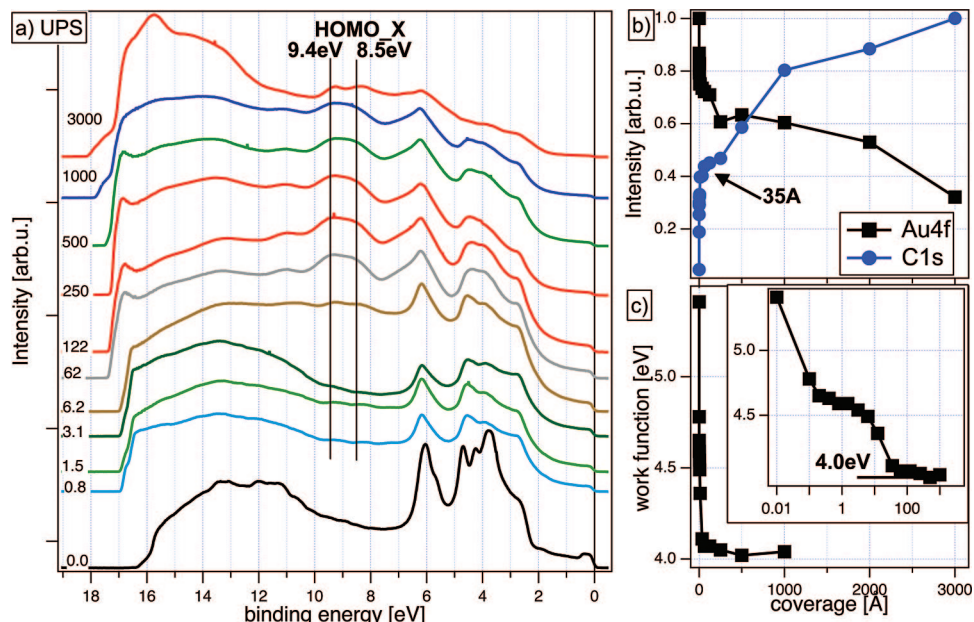


Figure 4. (a) Selected UPS spectra during the deposition of chrysene onto Au(111); (b) Integrated area XPS intensities and (c) work function change from the pure Au(111) surface toward the surface covered with chrysene (the inset shows the trend on a log scale).

splitting of 0.9 eV, equivalent to the separation observed for chrysene on Au(111) and HOPG. With the knowledge of the energy difference between HOMO_X and the HOMO cutoff (6.9 eV, see Figure 10c), a binding energy of the HOMO cutoff of 1.8 eV can be calculated.

Since the C 1s binding energy is constant, band bending in the chrysene layer can be excluded and confirmed by the constant binding energy for the HOMO_X emissions at coverages lower than 90 Å. Assuming a work function for the thick chrysene film of ≈4.0 eV (Au(111) and HOPG), a band energy diagram can be drawn as shown in Figure 13b.

Another interesting observation is the different shape of the HOMO_X emission in comparison with Au(111). On Cu(111)

the splitting is easily visible, as on HOPG (see Figure 10a), whereas on Au(111) the splitting is discernible only at high coverages (3000 Å) or near monolayer coverage (6.2 Å). The different shape of the HOMO emissions indicate a different chrysene morphology since photoemission spectroscopy is sensitive to emission angles. The different shape of the HOMO_X emission feature will be discussed in detail in Discussion Section.

C. Deposition onto Ag(111). The XPS and UPS spectra obtained during the growth of chrysene on Ag(111) are shown in Figures 7 and 8. Films thinner than 200 Å show a constant binding energy for the Ag 3d_{5/2} emission. The increase in Ag 3d_{5/2} binding energy at higher coverages is due to charging and

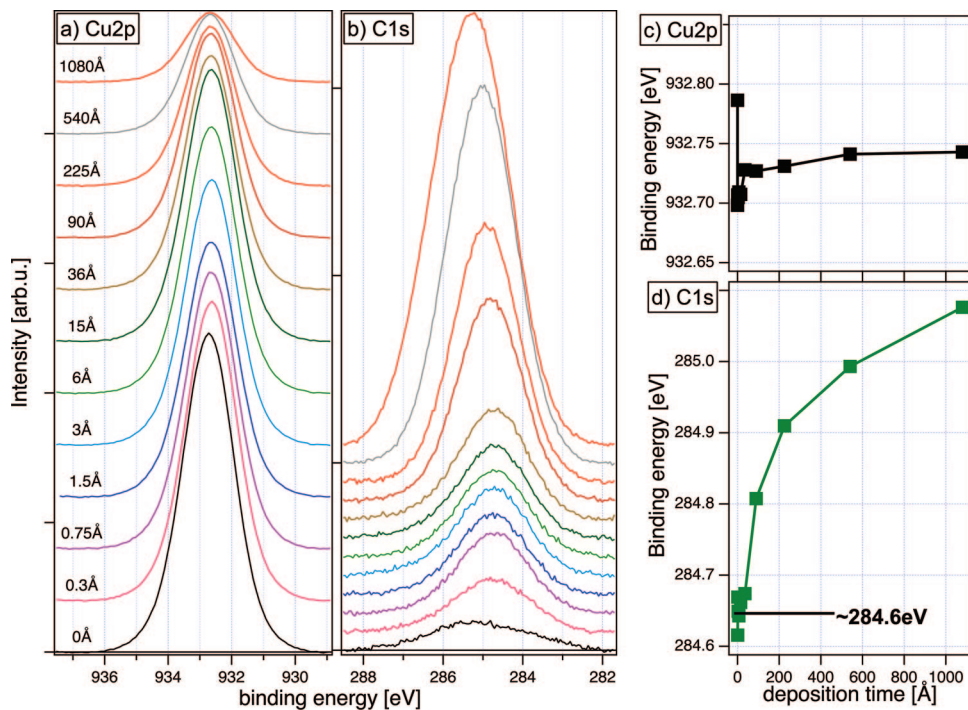


Figure 5. XPS spectra collected during the stepwise deposition of chrysene onto Cu(111): (a) Cu 2p_{3/2}, (b) C 1s. The binding energies for the Cu 2p and the C 1s determined by curve fitting procedures are given in (c) and (d), respectively.

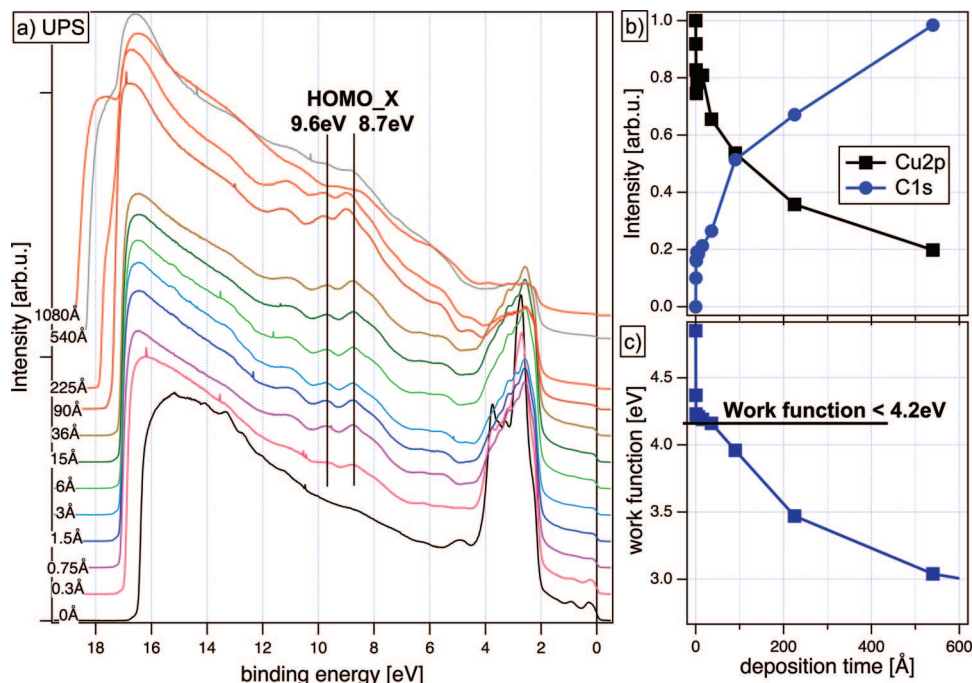


Figure 6. (a) UPS spectra obtained during the deposition of chrysene on Cu(111). (b) Intensities determined from the XPS measurements. (c) Change in work function as a function of deposition time.

is of the same order of magnitude as the increase in binding energy for the C 1s emission at the same coverages. Initially a shift to higher binding energies is detected for the C 1s emission that is related to screening effects as discussed for Au(111). A binding energy of 284.68 eV was measured for an intermediate thickness chrysene film on Ag(111), again comparable to the values observed for the previously presented surfaces.

From the trend of the intensities determined from the XPS fitting procedures (see Figure 8b), the same Stranski-Krastanov growth mode occurs on Ag(111) as was previously presented. After $\approx 14 \text{ \AA}$ a kink is visible in the plot of Ag 3d and the C 1s

emission intensity versus thickness of the chrysene layer (Figure 8b). A wetting layer of chrysene is formed at thicknesses less than 14 \AA , followed by island growth.

The UPS spectra shown in Figure 8a were evaluated as described previously. The trend of the work function is given in Figure 8c. Beginning with the work function of bare Ag(111) of 4.5 eV, the work function levels out at a value of 4.0 eV for intermediate thickness films. This value is comparable to those obtained for Au(111) and HOPG.

The low binding energy HOMO levels are again difficult to evaluate due to overlap with the Ag 4d valence band states.³⁴

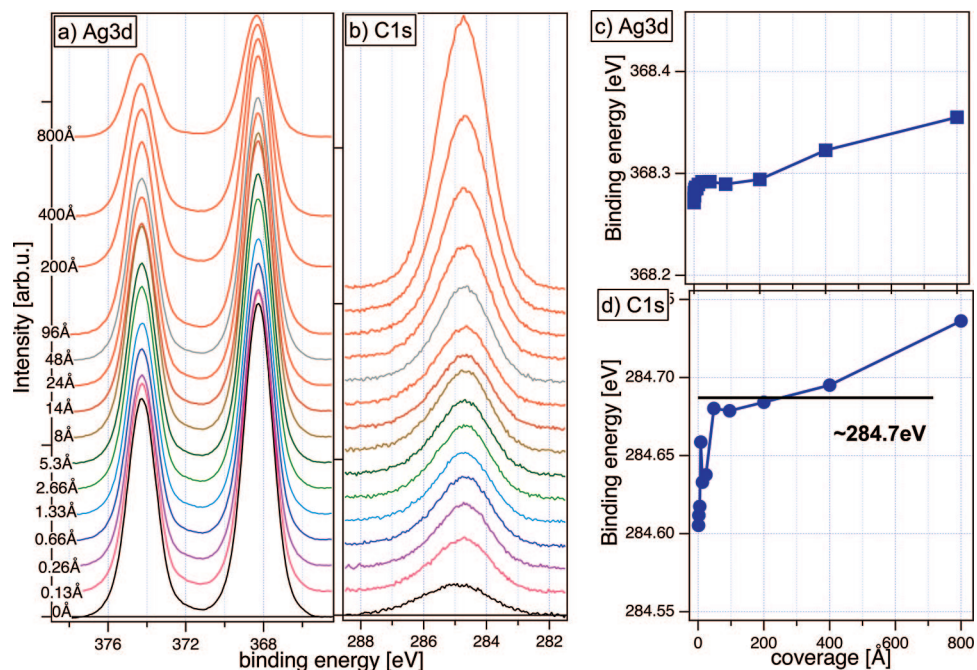


Figure 7. XPS spectra collected during the stepwise deposition of chrysene onto Ag(111): (a) Ag 3d, (b) C 1s. The binding energies for the Ag 3d_{5/2} and the C 1s determined by curve fitting procedures are given in (c) and (d), respectively.

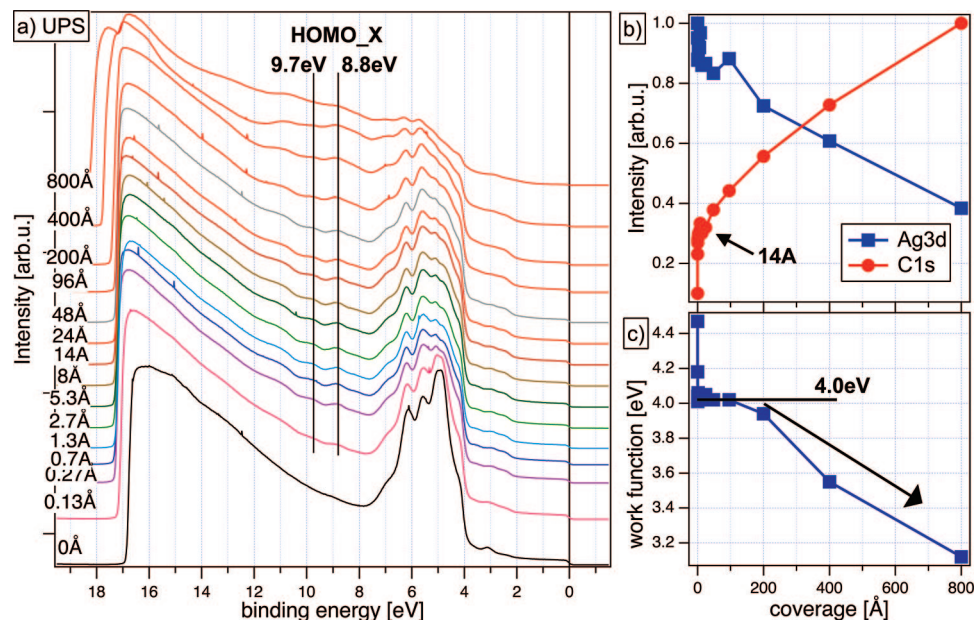


Figure 8. (a) UPS spectra obtained during the deposition of chrysene on Ag(111). (b) Intensities determined from the XPS measurements. (c) Change in work function as a function of deposition time.

Similar to Au and Cu in the region between 8 and 10 eV, there are no prominent substrate emissions, which allows for measurements of chrysene HOMO emissions in this region. The HOMO_X emissions are labeled in Figure 8a. The binding energy position of the low binding energy HOMO_X emission occurs at 8.8 eV, which allows for the determination of the HOMO cutoff position to be 1.9 eV. There are no detectable binding energy shifts in the HOMO_X emission, and therefore band bending can be excluded.

The shape of the HOMO_X is similar to that obtained for Cu(111) and HOPG indicating that chrysene grows on Ag(111) with a similar orientation as on Cu(111) and HOPG.

The measured work functions and the value for the binding energy of the HOMO cutoff allows for the construction of a

band energy diagram as shown in Figure 13c. The band gap of 3.4 eV obtained from UV-vis was used to determine the LUMO cutoff position. Due to the absence of band bending the obtained work functions directly translate into an interface dipole potential of $\delta = 0.5$ eV.

D. Deposition onto HOPG. Initially the binding energy of the C 1s on HOPG is approximately 284.7 eV and remains unchanged during the deposition of chrysene, as can be expected since both materials contain sp² hybridized carbon atoms (see Figure 9. The measured intensity of the C 1s emission is slightly reduced at long deposition times as a result of a lower density of carbon in the chrysene film in comparison to bulk HOPG which contains no hydrogen. The deposition of chrysene was continued until charging was apparent in the UPS.

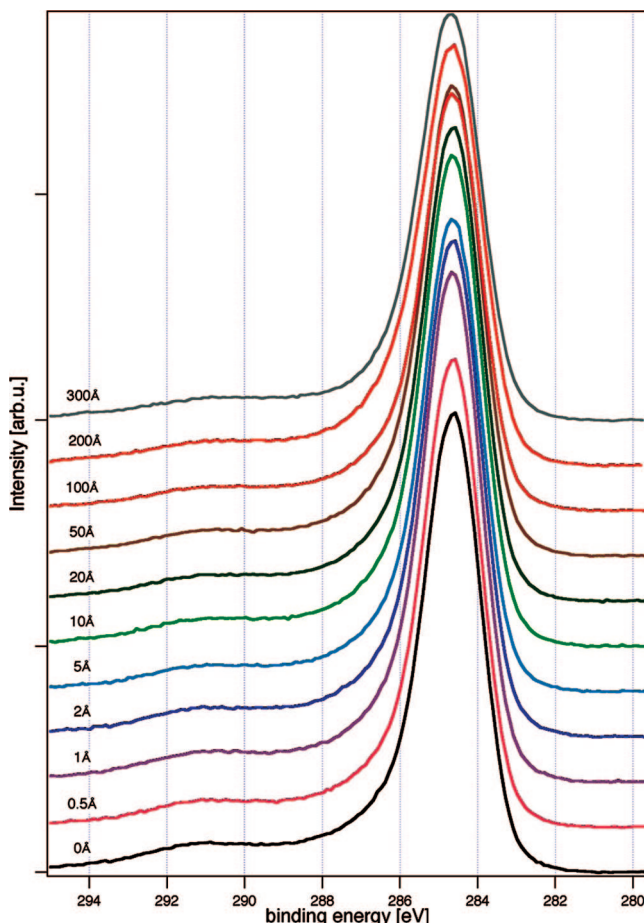


Figure 9. Collected XP spectra during the deposition of chrysene on HOPG. The binding energy remains unchanged at ≈ 284.7 eV.

The characteristic featureless UPS spectrum of HOPG below 11 eV is given in Figure 10a for 0 Å of chrysene.^{24,35,36} The bare HOPG UPS spectrum shows a well-known strong graphitic carbon related feature between 13 and 14 eV.³⁶ During the deposition of chrysene, the work function changed from 4.4 eV for the bare HOPG to 4.0 eV for the thick chrysene film as is shown in Figure 10b. For films thicker than 50 Å, charging occurred, manifested in a shift to higher binding energies of the SEO as well as the broadening of HOMO emissions. UPS spectra of films thicker than 200 Å are completely featureless.

No binding energy shifts in HOMO emissions were observed during the deposition of chrysene on HOPG, again in agreement with the unshifted position of the C 1s core level emission. In agreement with the other metallic substrates, band bending does not occur on HOPG. Due to the similar chemical environment for carbon atoms, bond screening effects will only play a minor role in the case of chrysene on HOPG, in agreement with the constant binding energy measured for the HOMO and the C 1s emissions.

The absence of strong emissions from HOPG in the binding energy range below 11 eV enables the determination of the HOMO cutoff position for chrysene. Immediately after the first deposition step (see Figure 10a) a number of new emissions appear that grow only slightly after the initial deposition step and exhibit no shape change for films up to 50 Å thick. A close examination of the photoemission onset allows for the determination of the HOMO cutoff position at a binding energy of 1.9 eV (see Figure 10c). In the experiments on Au(111), Cu(111), and Ag(111) the first HOMO emissions of chrysene overlap with metal valence band states. However, some chry-

sene-assigned HOMO states were visible for the metal substrates, and these are also labeled as HOMO_X in the spectra collected on HOPG. Since the molecule's HOMO emission energies do not change on the different substrates, the difference between the first HOMO_X emission and the HOMO cutoff is constant and was determined as 6.9 eV. As previously mentioned, this value was used to calculate the HOMO cutoff position of the metal substrates.

The electronic properties of chrysene on HOPG can be summarized in a band energy diagram given in Figure 13d. From the experimental data, an interface dipole potential of 0.4 eV is present at the interface between chrysene and HOPG. The LUMO cutoff position was again calculated by applying the UV-vis determined optical band gap.

E. Deposition onto SnS₂(0001). The last substrate in this study is a semiconductor with an indirect band gap of 2.2 eV.³⁷ Similar to HOPG, SnS₂ has a layered structure consisting of stacks of S–Sn–S atoms. At the surface no dangling bonds are present resulting in a van der Waals like surface, also similar to HOPG. Therefore only weak interactions between SnS₂ and chrysene can be expected. The surface is composed of hexagonally closed packed sulfur atoms giving this substrate the same hexagonal symmetry as the other metallic substrates discussed earlier.

Chrysene was deposited on SnS₂ with the same stepwise procedure as described previously. The collected XPS spectra are shown in Figure 11, panels a–c, for the Sn 3d, S 2p, and the C 1s core level emissions, respectively. During the deposition of chrysene, the binding energies of the substrate (Sn 3d in Figure 11d and S 2p in Figure 11e) remained nearly unchanged. During initial deposition steps, the binding energy of the C 1s core level emission of chrysene showed no significant changes (Figure 11f). Interestingly the C 1s binding energy obtained for chrysene on SnS₂ is 284.4 eV, about 300 meV smaller than those for the other substrates; this difference will be addressed later. Charging also occurs for films thicker than 60 Å leading to an observed increase in binding energy. As first mentioned in the section with the interface of chrysene to gold, a shift to higher binding energy for the C 1s core level emission was observed for all chrysene films investigated in the study. To confirm that the observed shifts were related to charging effects, the binding energies were measured as a function of the excitation intensity. In the case of SnS₂, the C 1s core level emission illustrated in Figure 11c shifted to higher binding energies at film thicknesses greater than 60 Å. Thus, charging effects were observed for the C 1s core levels as well as in the UPS in a more drastic manner than on the metallic substrates.

The trend of the XPS core level intensities is shown in Figure 12b. At a film thickness of approximately 24 Å, a kink occurs indicating a change of growth mode (indicating that Stranski–Krastanov growth mode also applies on SnS₂). Similarly, it was also not possible within reasonable deposition times/nominal film thicknesses to achieve a 100% suppression of substrate signals on SnS₂.

The UPS spectra collected after each deposition step are shown in Figure 12a. The work function, shown in Figure 12c was determined from the SEO. Initially a large shift to smaller work function values is clearly visible (from 5.2 eV of SnS₂ to 4.6 eV). This is probably the result of a semiconducting substrate with a lower conductivity, resulting in charging occurring at smaller film thicknesses. This makes the determination of the real work function of chrysene on SnS₂ very difficult and unprecise. In Figure 12c a kink in the evolution of the work function is visible (labeled with A). This kink indicates the

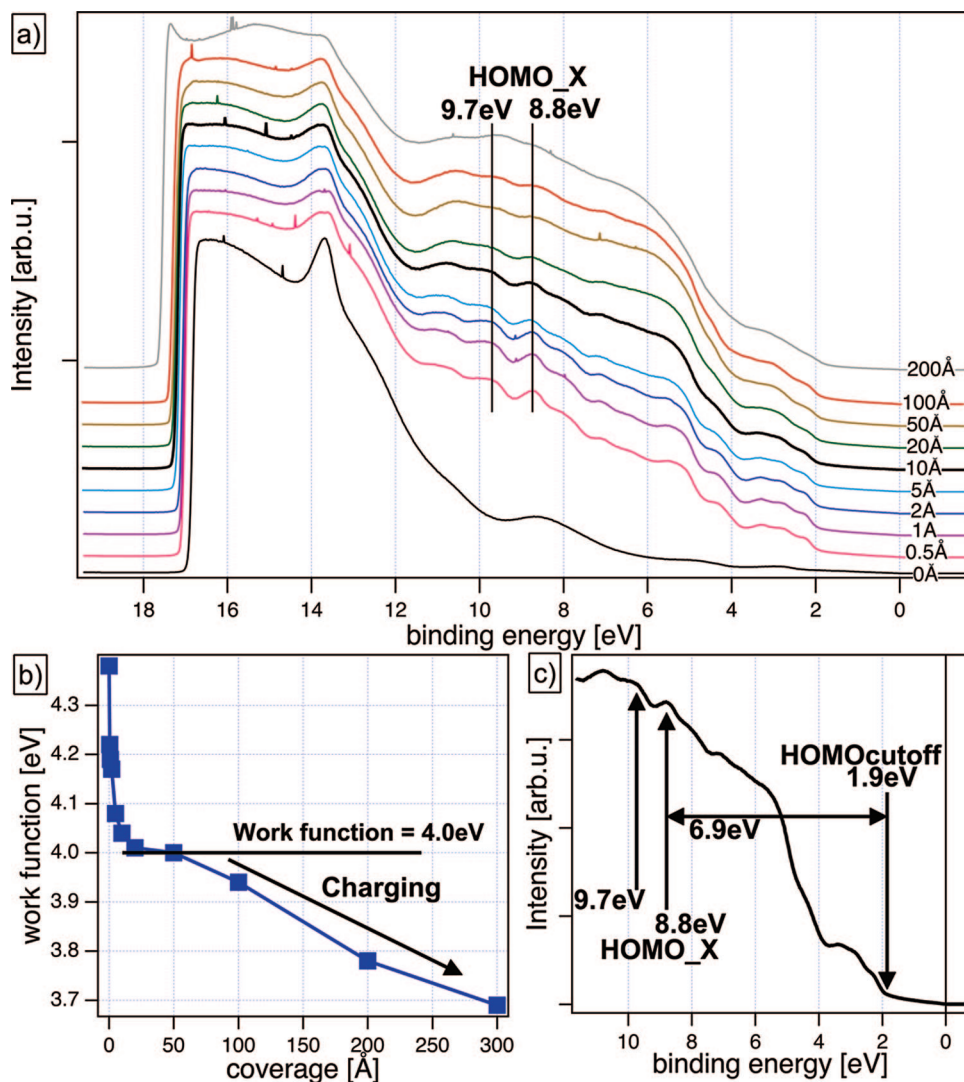


Figure 10. (a) UPS spectra collected during the deposition of chrysene onto HOPG. (b) Trend of the work function as function of deposition time and (c) a close-up of the HOMO_X region and the HOMO cutoff.

beginning of charging in the UPS spectra. Usually the work function of the overlayer should level out to a constant value (see, e.g., Figure 4c). As a guide for the eye, an arbitrary leveling off energy is indicated by the dotted curve in Figure 12c, leading to an approximate work function value of 4.4 eV for chrysene on SnS₂. This value is in reasonable agreement with the obtained difference for the HOMO_X and the C 1s emission when compared to experiments on the other substrates. For coverages thicker than 240 Å, the SEO is broadened and shows two SEOs.

SnS₂ exhibits a strong valence band emission in the range of 1.5–4.5 eV (composed of s and p states from Sn and S),³⁸ making the direct determination of the HOMO cutoff impossible. In the range between 5 and 11 eV, there are only very weak SnS₂ emissions that allow use of the same procedure as for the metallic substrates. The position of the HOMO_X emission is indicated by the two vertical lines in Figure 12a. Initially the two emissions from HOMO_X are clearly visible, but for coverages of more than 4 Å, the separate peaks merge into a broad emission for the thicker films. This emission reflects that obtained on Au(111), leading to the conclusion that the initial adsorption geometry is most likely planar with a transition to tilted molecules at film thicknesses of about 4 Å (\approx 1 monolayer).

The HOMO_X binding energy was determined to be 8.4 eV with an energy difference of 0.9 eV with respect to the second

feature, which is in agreement with the other substrates. Using the HOMO_X position, we calculate a HOMO cutoff position of 1.5 eV with respect to the Fermi level. The interface properties determined from the XPS and UPS measurements are summarized in the band energy diagram given in Figure 13e. With the knowledge of the energy position of the valence band maximum (1.8 eV, determined from a clean SnS₂ sample with UPS), the literature band gap of 2.2 eV for SnS₂,³⁷ the negligible change in Sn 3d and S 2p binding energy, and the initial work function of 5.2 eV, the SnS₂ side of the interfacial band energy diagram can be drawn. The chrysene side is determined by the calculated HOMO cutoff position and the approximate work function of 4.4 eV for a thick film as well as the optical band gap of 3.4 eV to determine the LUMO cutoff position. From these values an interface dipole potential of 0.8 eV can be calculated. For all other interfaces, the distance between HOMO cutoff and Fermi level describes the barrier for hole injection. Since SnS₂ is a semiconductor, the discontinuity between valence band maximum (VBM) and HOMO cutoff controls charge carrier transport. From the HOMO cutoff to the VBM, a discontinuity of $\Delta_{\text{VBM}}^{\text{HOMO,cutoff}} = 0.3$ eV is present.

IV. Discussion

The coverage dependent photoemission results for chrysene deposited onto the substrates studied herein consistently dem-

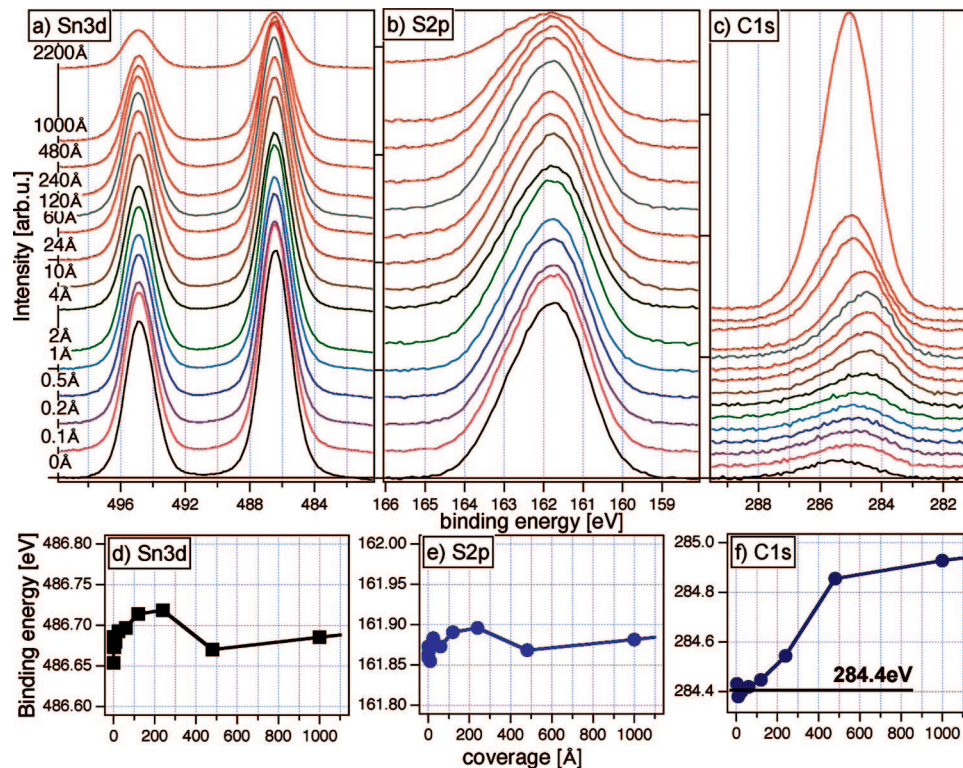


Figure 11. XPS spectra collected during the stepwise deposition of chrysene on SnS_2 : (a) Sn 3d, (b) S 2p, and (c) C 1s detail spectra. The determined binding energies are given in (d) for Sn 3d, (e) S 2p, and (f) for the C 1s emission.

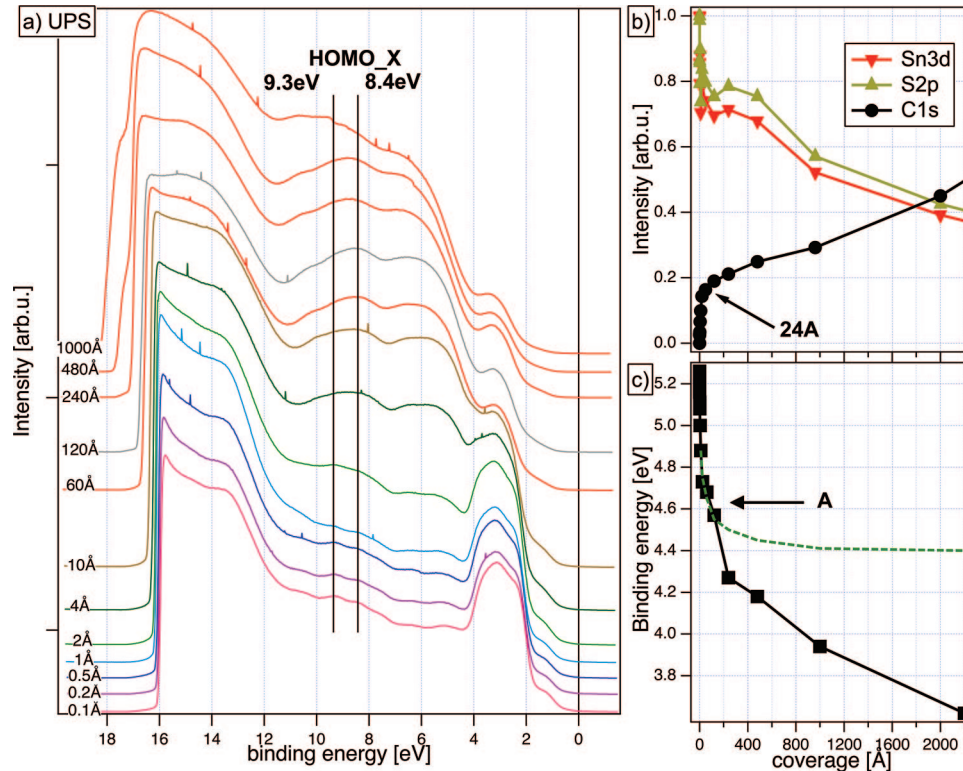


Figure 12. (a) UPS spectra obtained during the deposition of chrysene on SnS_2 . (b) Intensities determined from the XPS measurements. (c) Change in work function as a function of deposition time.

onstrate a wetting layer of chrysene is initially formed, followed by island growth (classic Stranski-Krastanov growth mode). Optical microscopy of the thickest films also shows clear evidence of large chrysene islands being formed (see chrysene on Ag(111) Figure 14a). The formation of large islands explains why it was not possible to fully suppress the substrate core level

photoemission signals. Therefore, regions with less than 3–4 ML (approximate escape depth of photoemitted electrons) must exist even for 100 nm thick chrysene films. Therefore, the wetting layer most likely contains only a monolayer of chrysene.

Evaluation of chrysene HOMO levels in the low binding energy region (0–7 eV) of the UPS spectra observed on Au,

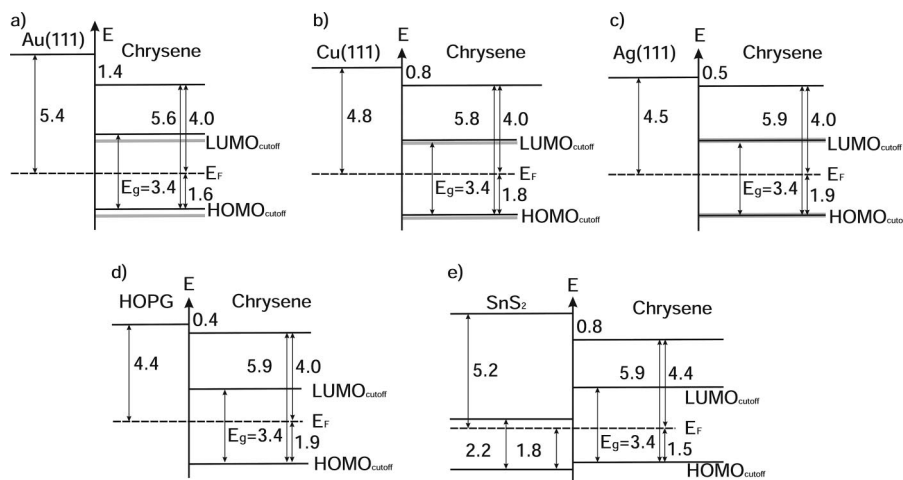


Figure 13. Band energy diagrams of the studied interface between chrysene and (a) Au(111), (b) Cu(111), (c) Ag(111), (d) HOPG, and (e) SnS₂. The gray indicated HOMO/LUMO levels show the levels, corrected from screening effects (see Discussion).

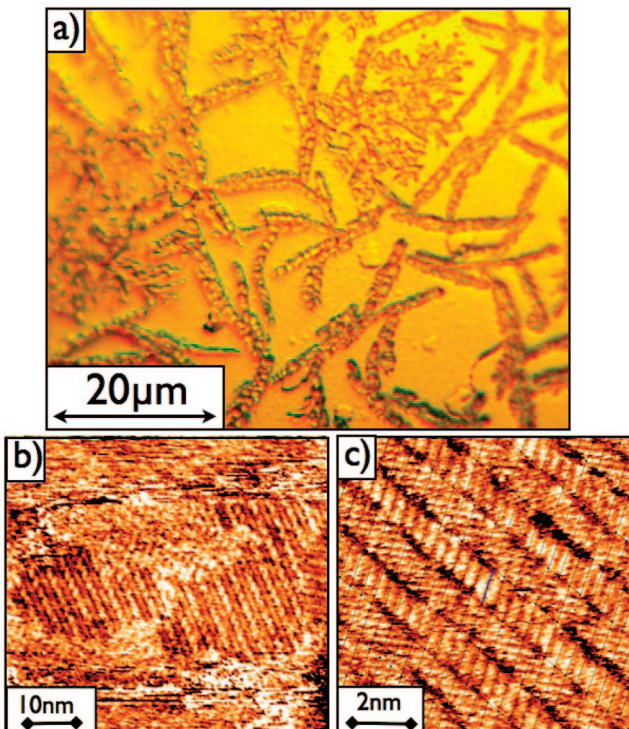


Figure 14. (a) Optical microscope image of a thick chrysene layer on Ag(111). (b and c) STM images (1.8 V, 0.20 nA) obtained in some areas of a 30 Å thick chrysene film on Au(111). The periodicity suggests that the molecules are tilted along their long side on the surface.

Ag, and Cu were convoluted due to the intense valence band emissions from the metal substrates. However, in the region of 8–10 eV, distinct chrysene HOMO emissions were observed on all metallic substrates upon the first deposition step and maintained a consistent value with all subsequent deposition steps. In addition, XPS results of the chrysene C 1s core level emission on all metallic substrates showed no shifts in binding energy, thus providing no evidence of band bending in the organic semiconductor. Since the energy difference between the two HOMO_X emissions (≈ 0.9 eV) was constant during each deposition step for each metallic substrate, the energy difference (≈ 6.9 eV, see Figure 10c) between the low binding energy HOMO_X emission and the HOMO cutoff position observed on HOPG, which shows no strong substrate states in the low binding energy region, was used to calculate the HOMO cutoff

position on Au, Ag, and Cu. This argument is supported by the lack of any energy shifts observed in either the XPS or UPS data, and the energy difference between the HOMO_X and HOMO cutoff on HOPG is regarded as a material property of chrysene.

Despite the fact that the binding energies and the energy splittings are very similar, there exist some differences between the substrates. A comparison between the chrysene HOMO_X emissions on Au(111) (see Figure 4a) and, e.g., HOPG (see Figure 10a) demonstrate some significant differences. On HOPG two distinct chrysene emissions are visible whereas on Au(111) only a broad two component peak is present. Since photoelectron emission is sensitive to the relative orientation of the molecules with respect to the analyzer, the different shapes of the emission spectra provides some indication of dissimilar alignment of the molecules on the various surfaces. Florio et al.³⁹ demonstrated via STM that chrysene lies flat on the HOPG surface in the submonolayer and monolayer regime. This leads to the conclusion and to our assumption for the following discussion that, if the HOMO_X is visible as two distinct emissions, chrysene is lying flat on the surface. On the low work function substrates, HOPG, Ag(111), and Cu(111), chrysene adsorbs flat on the surface whereas in the case of high work function materials such as SnS₂ and Au(111) the orientation of the molecules on the surface is best described as tilted due to the observed very broad HOMO_X emission. To check this conclusion, some preliminary STM images of chrysene on Au(111) were obtained (see Figure 14, panels b and c). An evaluation of these images shows that a herringbone-type structure is formed with a short 2D cell parameter of 4.6 Å and a long parameter of ≈ 26 Å. The short axis (≈ 4.6 Å) of the 2D unit cell (see overlaid black lattice in Figure 14c) indicates that the molecules are tilted along the long axis of the chrysene molecule since the short axis is less than that for tetracene and pentacene which have a width of ≈ 5.3 Å. These cell parameters give some evidence that the assumption to correlate the shape of the HOMO_X emission is somehow useful to roughly predict the orientation of the molecule on the surface. In-depth structural information via STM imaging at low temperatures will elucidate the tilt angle and 2D morphology since chrysene is highly mobile at room temperature (Florio et al. imaged chrysene on HOPG at 80 K).³⁹

The experimental results of the electronic interface properties will now be discussed. Jaegermann et al.⁶ have shown that barrier heights produced by metal deposition on nearly defect free van der Waals surfaces, such as WSe₂, approach the

Schottky limit. These materials show a slope of ≈ 1.0 for the change in barrier height with a change of the metal work function. The same plot for a covalently bonded semiconductor, e.g., silicon, shows a slope of only ≈ 0.1 , approaching the Bardeen limit as a result of Fermi level pinning. A survey of interface behavior and slope parameter as a function of the ionicity of the semiconductor was first given by Kurtin et al.⁴⁰ These findings are explained partly by the concepts of metal-induced gap states (MIGS)^{3,5,41} and the presence of interfacial gap states.^{2,9} The interfacial states (roughly one to two states per interfacial atom), are usually located in the band gap region of the semiconductor and lead to the concept and the definition of a charge neutrality level E_{CNL} (early calculations were done by Cardona et al.)⁴² that are only slightly changed by metal adsorption onto the semiconductor. Therefore the Fermi level is almost pinned at E_{CNL} , which results in the small slope values ($S \approx 0.1$). From this inorganic semiconductor approach, the behavior of organic molecules on metals should be analogous to layered materials due to the absence of any strong chemical interactions and the presence of only weak van der Waals forces. Thus organic materials should approach the Schottky limit. Evidently this is not the case. For pentacene, XPS and electrical measurements have shown^{27,30,31} that the barrier height changes with metal work function with a slope of only 0.36. Kahn et al.²⁷ have provided examples of S values for other planar molecules which never exceeded the value for pentacene, e.g., ZnPc $S = 0.25$, PTCDA $S = 0.0$, or PTCDI $S = 0.0$. The last two examples showed a slope of 0.0, demonstrating pure Fermi level pinning.

As discussed briefly for the Au(111)/chrysene interface, the initial increase in C 1s binding energy can be explained by a reduction of screening effects in the growing chrysene film.^{23–29} The morphology of the thick chrysene films studied on the substrates herein, as illustrated by the optical microscope images in Figure 14, is glaringly inhomogeneous. As a result, a reduction of screening effects are only manifested in regions of the sample exhibiting island morphology. Our XPS results indicate the initial increase in C 1s binding energy; however no measurable shift was observed for the HOMO_X emissions in the UPS spectra. From the escape depth of photoexcited electrons (C 1s $\approx 20 \text{ \AA} \approx 3–4 \text{ ML}$) it is understandable that the majority of the XPS signal mainly originates from the bulk and includes surface island regions, here from the chrysene islands. We therefore believe the XPS measurements more accurately reflects bulk (island) properties of the thick chrysene film, whereas monolayer regions of the chrysene film are probed by UPS and demonstrate no dependence on screening length. To comment on the different coverage where charging occurs, it has to be mentioned that the light intensity during UPS is much higher than in the XPS measurement. From that point of view, it is understandable that charging becomes observable in UPS measurements. The HOMO emissions which do not show any appreciable shift in binding energy more accurately reflect photoelectrons escaping from well-ordered monolayer regions of the sample, as shown in STM images in Figure 14. Photoelectrons excited from HOMO levels of chrysene molecules from the islands will show energy shifts due to charging and will only lead to a broadening of the spectrum (increased background) on the high binding energy side.

The secondary electron onset on the other hand probes predominately the islands (due to the high number of secondary electrons generated in the chrysene film and due to their large escape depth) and more accurately measures the work function of thick chrysene films (or more precisely the islands). This is

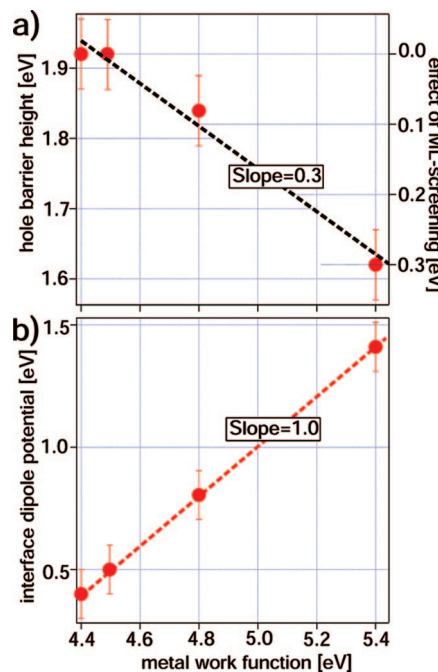


Figure 15. (a) Plot of the hole barriers (left scale) from the band energy diagrams in Figure 13. The right axis label indicates the screening effect that leads to the conclusion of a constant barrier height. (b) Plot of the obtained interface dipole potential δ as a function of the metal work function. (a) and (b) only contain the investigated metals, not the semiconducting substrate SnS₂.

also in agreement with similar values obtained for the C 1s core level emission and the measured work function for chrysene. Considering the ionization potential of chrysene to be a property of the molecule, the band energy diagrams as represented by the black lines in Figure 13 are incorrect. The ionization potential (left side of y axis on the chrysene interface) changes with metal work function because the HOMO cutoff position changes. The slope of the change in HOMO cutoff position, equivalent to a change in hole barrier height, is 0.3 (see Figure 15a). As mentioned previously, we believe the HOMO emissions are exemplary of monolayer regions and thus we cannot interpret this observation as a change in barrier height. More accurately this change in binding energy demonstrates a change of the screening strength of the metallic substrate at monolayer coverages (right y axis label in Figure 15a).

Since there were no detectable energy shifts in either the C 1s core level emission or the HOMO positions in the HOPG experiment, we can assume that interface screening effects do not play an important role in this system. Therefore the band energy diagram for the HOPG/chrysene interface (see Figure 13d) can be assumed to accurately reflect the system and serves as a reference. For Au(111), Cu(111), and Ag(111) a similar C 1s binding energy was observed, and therefore the HOMO cutoff for these interfaces must occur near 1.9 eV as indicated by the gray bars in Figure 13, panels a–c. This results in a constant ionization potential and to a conclusive picture of these interfaces.

These findings lead to the conclusion that the interface dipole potential δ depends on the work function of the substrate whereas no barrier height changes occur when varying the work function of the substrate (see Figure 15b). This is the Bardeen limit for Schottky barriers, and the Fermi level in the semiconductor (here chrysene) is completely pinned. Vázquez et al. calculated the slope parameters S in terms of effects that are most dominant at organic/metal interfaces.^{43,44} They embedded

TABLE 1: Experimentally Obtained Electronic Properties of Pentacene and Chrysene^a

	pentacene	chrysene
structural formula	C ₂₂ H ₁₄	C ₁₈ H ₁₂
molecular weight	278	228
slope parameter	0.36	0
ionization potential [eV]	4.9	5.9
band gap [eV]	1.85	3.4
HOMO		

^a The last row displays the calculated HOMO localization for pentacene vs chrysene.

in their calculation the so-called *pillow effect* which accounts for the adsorbate-induced change of the substrate work function, where typically a lowering of the metal work function is observed. Furthermore they include in their model a charge transfer to the substrate induced states in the organic semiconductor. This induced density of interface states leads to the IDIS (induced density of interface states) model that describes metal states tailing into the semiconductor. This tailing of metal states into another material is also termed metal-induced gap states (MIGS theory). From their conclusion the *pillow effect* only plays a minor role while the IDIS effect mainly influences the slope parameter for Schottky barriers. If the IDIS effect is high, the Fermi level of the organic semiconductor will be pinned close to the charge neutrality level. Since this is the case for metal/chrysene interfaces, we can experimentally determine the charge neutrality level for chrysene with respect to the HOMO cutoff position. The charge neutrality level within this model of chrysene is 1.9 eV above the HOMO cutoff, slightly above mid band gap of chrysene using the optical band gap as a first-order approximation.

The results obtained for chrysene on the various metals demonstrate that the Fermi level is pinned. Chrysene is a planar π -conjugated PAH similar to pentacene; however there are several structural differences between the molecules (number of C atoms, 2D geometry, HOMO–LUMO gap). From this point of view one would expect a similar behavior in the electronic interface properties of the two molecules. Evidently this is not the case: chrysene shows Fermi level pinning ($S = 0$) whereas pentacene demonstrates a slope parameter of $S \approx 0.36$.^{27,28,30,31} The question arising from these observations is as follows, what are the fundamental properties of a molecule that primarily determine the electronic properties of the interface? In Table 1 a list of experimentally determined properties for chrysene and pentacene is given. The ionization potentials and band gaps are quite different. The band gap influences the tailing of the induced metal states into the band gap region of

the organic molecule as calculated by Chem3D. But the local electronic structure of the molecule will also influence the tailing. The last row in Table 1 shows the difference in the HOMO orbital distribution for the two molecules. The HOMO contour plot for pentacene shows five regions of high π -electron density located (as it can be expected) around the five rings in pentacene. Therefore a HOMO with π -electron density centered at the four rings of the chrysene molecule might be expected. Surprisingly this is not the case. The calculation for chrysene with the same settings to display the HOMO shows only three areas which are not correlated to the location of the benzene rings in chrysene. From this standpoint we can speculate that the molecular alignment with respect to the substrate and the local position of the HOMO/LUMO states play an important role in the controlling the interfacial behavior between metals and organic materials. To investigate this hypothesis, a detailed study of the different structural isomers, such as tetracene and triphenelyene in comparison with chrysene, would be very interesting.

There is also an opportunity for theoretical studies that consider the atomic level physical and electronic structure of the interface rather than bulk properties, such as work function and band gap, to shed light onto this interesting issue. In terms of electronic properties, one must consider the difference between semiconductors and insulators. Both are commonly described by a band gap with a defined value. However the band gap alone does not provide complete understanding of the electronic properties of semiconductors versus insulators. More importantly is the issue of electronic transport properties of holes or electrons. An analyses of charge hopping processes from one molecule to another must be studied additionally. Future investigations should be directed not only to the interaction between neighboring π orbitals from one molecule to the next but also to the interaction between the π states of the organic molecule and the substrate (here a metal). Recently Ferretti et al.⁴⁵ and Yamane et al.⁴⁶ introduced a new concept of mixing metal states with π states of the adsorbed organic molecule. This interaction can be understood as a quasi-hybridization between organic π states and metal states. This mechanism forms new states inside the band gap of the organic semiconductor and pins the Fermi level to a certain energy level. Most significantly the pinned energy level is a property of both the metal and the organic, not a property of the semiconductor alone.

For future theoretical investigations, it is always helpful to reduce the number of variables—here reducing the number of orbitals and electrons to include the first run of calculations. In this study the highest metal states result from s states. Therefore it is most likely that the metal s states will primarily interact with the organic π states. There are two indications that strengthen this conclusion: (1) the prominent d states are only slowly suppressed as one can expect from the subsequent increase of a growing overlayer and (2) the interesting fast suppression of the surface state (see Au(111) in Figure 4 and for Cu(111) in Figure 6). This surface state is suppressed completely after the deposition of $\approx 0.8 \text{ \AA}$ equal to far less than a quarter monolayer of chrysene. This demonstrates, that near surface and surface states are the most crucial states to include in a detailed theoretical investigation. For the metal/chrysene interfaces studied herein, the most important interaction is between metal s states and organic π states, which in terms of the Ferretti et al. and Yamane et al.^{45,46} approach involves the hybridization between metal s states and organic π states.

SnS₂ behaves slightly differently due to its different electronic properties. Although the substrate symmetry is the same as that

of the metals, the semiconductor properties lead to different interfacial effects. The dielectric constants for SnS_2 and chrysene are most likely very similar ($\epsilon \approx 5-10$) and therefore screening effects play only a minor role in $\text{SnS}_2/\text{chrysene}$ junctions. Since SnS_2 was the only semiconductor studied herein, no general conclusions may be derived for the alignment of the conduction band minimum/valence band maximum with the LUMO/HOMO. Further work must be done to obtain a detailed description of semiconductor/chrysene junctions.

V. Conclusions

The present work demonstrated that the injection barriers for either holes or electrons of metal/chrysene interfaces do not depend on the work function of the metal. The metal/chrysene interfaces show complete Fermi level pinning where any change in work function of the metal does not change the barrier height. UPS measurements, in combination with the optical band gap of chrysene, reveal that the Fermi level is pinned at the charge neutrality level at ≈ 1.9 eV above the HOMO cutoff position, placing the Fermi level slightly above mid band gap.

The UPS and XPS spectra indicated that a wetting layer of chrysene is formed on all substrates, followed by island growth. The different binding energies obtained for HOMO_X on different substrates are a result of the different screening strengths for the different materials where a linear relationship between screening strength and work function of the metal was found.

The experimental results were discussed with respect to the most recent theories toward gaining a better understanding of metal/organic interfaces. The results provide certain indications that the interaction can be understood via a hybridization mechanism between metal states and organic π states.

The different observed shapes of the HOMO_X emissions provides strong evidence for different molecular alignments on the surface. Since chrysene is only 2D chiral, tilted molecules cannot form chiral domains and it is therefore very unlikely that chrysene will form stable chiral domains on either substrate. The visible splitting of the HOMO_X on HOPG is an indication for flat-lying molecules.³⁹ Following this interpretation, chrysene is flat-lying on the lower work function materials HOPG, Ag(111), and Cu(111) and most likely tilted on Au(111) and SnS_2 .

Acknowledgment. This work was supported by NSF Grant No. CHE-0518563.

References and Notes

- (1) Schottky, W. Z. *Phys.* **1939**, *113*, 367.
- (2) Bardeen, J. *Phys. Rev.* **1947**, *71*, 717.
- (3) Louie, S.; Chelikowsky, J.; Cohen, M. *Phys. Rev. B* **1977**, *15*, 2154.
- (4) Brillson, L. J. *Phys. Rev. Lett.* **1978**, *40*, 260.
- (5) Tersoff, J. *Phys. Rev. Lett.* **1984**, *52*, 465.
- (6) Jaegermann, W.; Pettenkofer, C.; Parkinson, B. A. *Phys. Rev. B* **1990**, *42*, 7487.
- (7) Tung, R. T. *J. Vac. Sci. Technol., B* **1993**, *11*, 1546.
- (8) Mönch, W. *Appl. Phys. Lett.* **1998**, *72*, 1899.
- (9) Tung, R. T. *Phys. Rev. Lett.* **2000**, *84*, 6078.
- (10) Gundlach, D. J.; Lin, Y. Y.; Jackson, T. N.; Nelson, S. F.; Schlom, D. G. *IEEE Electron Device Lett.* **1997**, *18*, 87.
- (11) Lin, Y. Y.; Gundlach, D. J.; Nelson, S. F.; Jackson, T. N. *IEEE Electron Device Lett.* **1997**, *18*, 606.
- (12) Lin, L.-B.; Jenekhe, S. A.; Young, R. H.; Borsenberger, P. M. *Appl. Phys. Lett.* **1997**, *70*, 2052.
- (13) Ishii, H.; Sugiyama, K.; Ito, E.; Seki, K. *Adv. Mater.* **1999**, *11*, 605.
- (14) Kang, J. H.; Zhu, X.-Y. *Appl. Phys. Lett.* **2003**, *82*, 3248.
- (15) Kang, J. H.; Zhu, X.-Y. *Chem. Mater.* **2006**, *18*, 1318.
- (16) France, C. B.; Schroeder, P. G.; Parkinson, B. A. *Nano Lett.* **2002**, *2*, 693.
- (17) France, C. B.; Schroeder, P. G.; Forsythe, J. C.; Parkinson, B. A. *Langmuir* **2003**, *19*, 1274.
- (18) Guaino, P.; Cafolla, A.; Carty, D.; Sheerin, G.; Hughes, G. *Surf. Sci.* **2003**, *540*, 107.
- (19) Guaino, P.; Cafolla, A. A.; McDonald, O.; Carty, D.; Sheerin, G.; Hughes, G. *J. Phys.: Condens. Matter* **2003**, *15*, S2693.
- (20) Lukas, S.; Witte, G.; Wöll, C. *Phys. Rev. Lett.* **2002**, *88*, 028301.
- (21) Chen, Q.; McDowall, A.; Richardson, N. *Langmuir* **2003**, *19*, 10164.
- (22) Söhnchen, S.; Lukas, S.; Witte, G. *J. Chem. Phys.* **2004**, *121*, 525.
- (23) Hill, I. G.; Mäkinen, A. J.; Kafafi, Z. H. *J. Appl. Phys.* **2000**, *88*, 889.
- (24) Schroeder, P. G.; France, C. B.; Parkinson, B. A.; Schlaf, R. *J. Appl. Phys.* **2002**, *91*, 9095.
- (25) Schroeder, P. G.; France, C. B.; Park, J. B.; Parkinson, B. A. *J. Phys. Chem. B* **2003**, *107*, 2253.
- (26) France, C. B.; Parkinson, B. A. *Langmuir* **2004**, *20*, 2713.
- (27) Kahn, A.; Gao, W. *J. Polym. Sci., Part B: Polym. Phys.* **2003**, *41*, 2529.
- (28) Watkins, N. J.; Yan, L.; Gao, Y. *Appl. Phys. Lett.* **2002**, *80*, 4384.
- (29) Amy, F.; Chan, C.; Kahn, A. *Org. Electron.* **2005**, *6*, 85.
- (30) Diao, L.; Frisbie, C. D.; Schroepfer, D. D.; Ruden, P. P. *J. Appl. Phys.* **2007**, *101*, 014510.
- (31) Jaeckel, B.; Parkinson, B. A. *Surf. Sci.* Submitted.
- (32) Shirley, D. A. *Phys. Rev. B* **1972**, *5*, 4709.
- (33) Qu, Z.; Ye, L.; Goonewardene, A. K.; Subramanian, M. N.; Karunamuni, J.; Strockbauer, R. L.; Kurzty, R. L. *J. Vac. Sci. Technol., A* **1994**, *12*, 2187.
- (34) Shevchik, N. J.; Liebowitz, D. *Phys. Rev. B* **1977**, *16*, 2395.
- (35) Schroeder, P. G.; Nelson, M. W.; Parkinson, B. A.; Schlaf, R. *Surf. Sci.* **2000**, *459*, 349.
- (36) Schlaf, R.; Parkinson, B. A.; Lee, P. A.; Nebesny, K. W.; Armstrong, N. R. *Surf. Sci.* **1999**, *420*, L122.
- (37) Aruchamy, A. *Photoelectrochemistry and Photovoltaics of layered Semiconductors*; Kluwer Academic Publisher: Dordrecht, Boston, and London, 1992; Vol. 14.
- (38) Simunek, A.; Wiech, G. *Phys. Rev. D* **1984**, *30*, 923.
- (39) Florio, G. M.; Werblowski, T. L.; Mueller, T.; Berne, B. J.; Flynn, G. W. *J. Phys. Chem. B* **2005**, *109*, 4520.
- (40) Kurtin, S.; McGill, T. C.; Mead, C. A. *Phys. Rev. Lett.* **1969**, *22*, 1433.
- (41) Heine, V. *Phys. Rev.* **1965**, *138*, A1689.
- (42) Cardona, M.; Christensen, N. *Phys. Rev. B* **1987**, *35*, 6182.
- (43) Vazquez, H.; Oszwaldowski, R.; Pou, P.; Ortega, J.; Perez, R.; Flores, F.; Kahn, A. *Europhys. Lett.* **2004**, *65*, 802.
- (44) Vazquez, H.; Dappe, Y. J.; Ortega, J.; Flores, F. *J. Chem. Phys.* **2007**, *126*, 144703.
- (45) Ferretti, A.; Baldacchini, C.; Calzolari, A.; Di Felice, R.; Ruini, A.; Molinari, E.; Betti, M. G. *Phys. Rev. Lett.* **2007**, *99*, 046802.
- (46) Yamane, H.; Yoshimura, D.; Kawabe, E.; Sumii, R.; Kanai, K.; Ouchi, Y.; Ueno, N.; Seki, K. *Phys. Rev. B* **2007**, *76*, 165436.